photonics

MDPI

Article

ZnO-Based Materials: From Pauli's Nonsense to a Key Enabling Technology

Juan Francisco Ramos-Justicia [1], Adalyz Ferreiro [2], Gregorio Flores-Carrasco [3], Sara Rodríguez-Cañamero [1], Ana Urbieta [1], María Eugenia Rabanal [2] and Paloma Fernández [1,*]

[1] Department of Physics of Materials, Faculty of Physics, University Complutense, Plaza de Ciencias 1, 28040 Madrid, Spain; juanfrra@ucm.es (J.F.R.-J.); sararc@ucm.es (S.R.-C.); anaur@ucm.es (A.U.)
[2] Department of Material Science and Engineering and Chemical Engineering, Carlos III University and IAAB, Avenida de la Universidad 30, 28911 Leganés, Spain; adferrei@ing.uc3m.es (A.F.); eugenia@ing.uc3m.es (M.E.R.)
[3] Tecnológico Nacional de México/ITS de Tepeaca, Tepeaca 75219, Mexico; flcagr@hotmail.com
* Correspondence: arana@ucm.es

Abstract: In this work, we aim to highlight the increasing interest in semiconductors, particularly ZnO. A revision of the evolution of the scientific production on three selected topics has been conducted. As an indicator of scientific production, the number of publications indexed in the Web of Science Data Base has been used. The search terms selected range from the general to the particular: semiconductors, oxide semiconductors, and ZnO. The period considered is from 1 January 1900 to 6 June 2023. The importance of doping processes in tailoring the properties of these materials, and the relevance of the most recently derived applications are also revised. Since many of the most recent applications that have been developed or are under development refer to optoelecronic properties, doping with rare earth elements has a central role. This was the reason behind choosing the system ZnO doped with Rare Earth elements (Eu, Gd, and Ce) and codoped with Ru to illustrate the materials' tuning potential of doping processes. Morphology, crystal structure, and luminescent properties have been investigated. Upon doping, both the Near Band Edge and the Deep Level emissions show a remarkable difference due to the change in the relative weight of the components constituting these bands. The spectra in all cases extend over the whole visible range, with a main emission in the violet-blue region corresponding to the Near Band Edge, and a broad band extending from the blue-green to orange-red region associated with the presence of different defects.

Keywords: semiconductors; oxides; ZnO

Citation: Ramos-Justicia, J.F.; Ferreiro, A.; Flores-Carrasco, G.; Rodríguez-Cañamero, S.; Urbieta, A.; Rabanal, M.E.; Fernández, P. ZnO-Based Materials: From Pauli's Nonsense to a Key Enabling Technology. *Photonics* **2023**, *10*, 1106. https://doi.org/10.3390/photonics10101106

Received: 22 June 2023
Revised: 30 August 2023
Accepted: 26 September 2023
Published: 30 September 2023

1. Introduction

In 1931, Wolfgang Ernst Pauli said to Rudolf Peierls:

"Über Halbleiter sollte man nicht arbeiten, das ist eine Schweinerei, wer weiss, ob es überhaupt Halbleiter gibt!"

That could be translated into "Nobody should work on semiconductors. It is a nonsense, who knows even if they exist!". Some years later, Georg Busch was told by his colleagues that "working on semiconductors was a scientific suicide" and "what are they good for? They are erratic and non-reproducible." Since these times, semiconductors have been revealed as key materials for most of the current technologies, but they remain among the most challenging materials. A non-exhaustive search in the Web of Science Data Base (Web of Science, June 2023) will confirm this idea about the role of semiconductors during the first half of the XXth century. Figure 1a shows the evolution of the number of publications produced since 1900 on the "Topic: Semiconductor" (the search has been completed with the single tag: semiconductor). According to the records recovered from this search, the first publications on semiconductors appeared between 1920 and 1940. From the 41 papers published in this period, only 5 appeared between 1928 and 1930

(1928, Annalen der Physik; 1929 Annalen der Physik; 1930 Annalen der Physik (2) and Zeitschrift für Physik (1)). Also very significant is the distribution of papers per category. In terms of the papers published between 1928 and 1940, the main category is "Physics Multidisciplinary" (Figure 1b), and in the last periods, the dispersion among categories is very large, with many of them being related to technology and applications (Figure 1c).

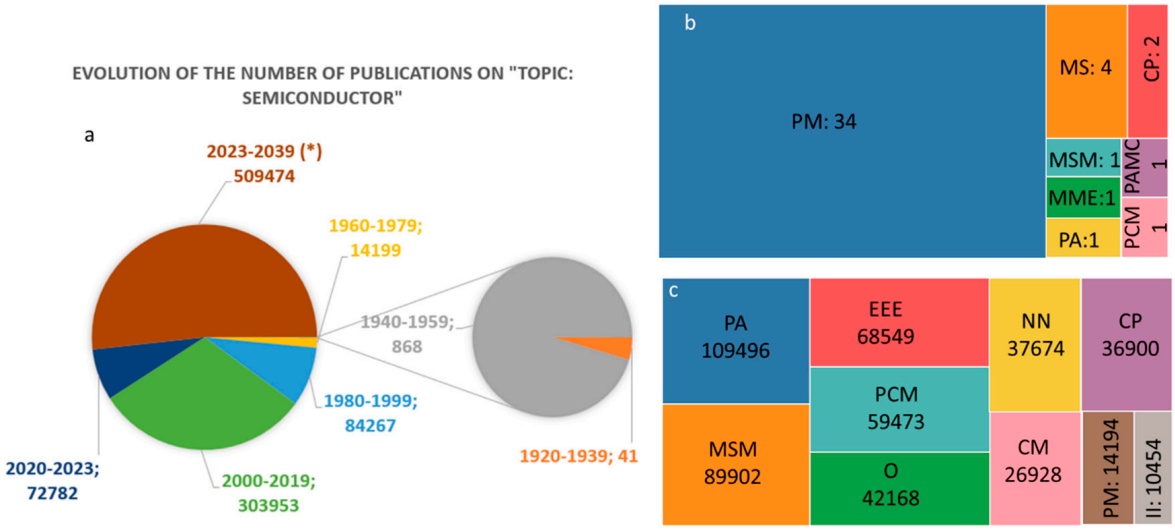

Figure 1. (**a**) Number of publications according to Web of Science Data Base on the search term "Semiconductors" from 1900 to date. * The number corresponding to 2023–2039 has been estimated as being proportional to the production in the period 2020–June 2023. Distribution among categories in the period (**b**) 1920–1940 and (**c**) 2000–2020: PM: Physics Multidisciplinary; MS: Multidisciplinary Sciences; MME: Metallurgy Metallurgical Engineering; PAMC: Physics, Atomic, Molecular, Chemical; PCM: Physics Condensed Matter; PA: Physics Applied; MSM: Materials Science Multidisciplinary; EEE: Engineering Electrical Electronic; CM: Chemistry Multidisciplinary; NN: Nanoscience Nanotechnology; CP: Chemistry Physical; II: Instruments Instrumentation; O: Optics.

Besides "traditional" semiconductors such as Si, Ge, or II-V compounds and their alloys, in recent decades, much interest has been shown in the study of semiconductor oxides. Metal oxides, either in bulk or as thin films or at the nanoscale, have a variety of properties that make them very multifunctional materials. The complexity of these materials may be seen simultaneously as a drawback or as an advantage. The drawbacks include how their properties depend strongly on crystal structure, stoichiometry, the presence of native defects, and doping, which are extremely difficult to control. The advantage is that if we learn how to control the main factors influencing the properties, we will be able to tune them over broad ranges, ensuring that the materials are suitable for applications in solar cells, gas sensors, photocatalysis, optoelectronic devices, and energy storage [1–11]. Figure 2 shows the results of refining the above search. If the search term "semiconductor oxides" is used, as expected, very few results are found before 1980. Between 1980 and 1999, only 6301 are reported by the Web of Science search engine, and over the next 20 years, 55,799 results are reported, almost a factor of 9, and the estimation for the current 20-year period is circa 130,000 publications.

Among semiconductor oxides, ZnO plays a central role and has been the focus of a great number of works. It is very difficult to pinpoint the first paper published on ZnO, but probably the first paper on ZnO that could be considered seminal is the work of Parsons and Crowther, published in 1917 in the Journal of American Chemical Society, entitled "Preparation and Properties of Zinc Oxide and Cadmium Oxide" [12]. In this paper, different synthesis routes for ZnO and CdO are described, and the physical and chemical properties (relevant at that time) were studied. In 1922, a work that could be considered the first paper to focus on the luminescent properties of ZnO was published.

The authors, Yoshio Haga and Eichi Haga, characterized the blue and green luminescence and designed some of the pioneering experiments to elucidate the origin of these emissions. The paper entitled "Über die Lumineszenz des Zynkoxyds" was published in Physikalische Zeitschrift [13]. For decades, the main applications of ZnO were related to phosphorescence. However, in the late 1960s, the non-linear electrical behavior of this material was first described. The authors, Cooper and Rhoderick, reported a voltage-dependent resistor (VARiable resISTOR) based on Cu-doped ZnO. This work [14] marked the beginning of the extensive study of ZnO-based varistors, and for about 30 years, this was one of the most relevant applications. However, during the last years of the XXth century, with the development of nanotechnology and optoelectronics, a bunch of ever-increasing new applications came into play, and the enormous potential of this material as a gas sensor, photocatalyzer, or as part of optoelectronic devices is being increasingly fostered every day [1,15–23]. This range of new applications is evident in Figure 3b, where areas such as "Energy fuels" (EF), "Environmental Sciences" (ES), and "Engineering Chemical" (EC) accumulate circa 6000 publications in the period 1 January 2020–6 June 2023.

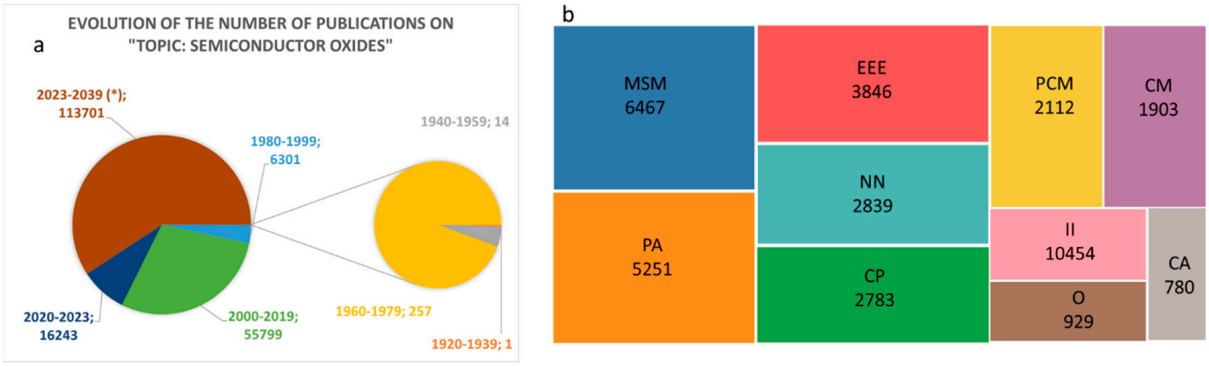

Figure 2. (**a**) Number of publications according to Web of Science Data Base on the search term "Semiconductor oxides" from 1900 to date. * The number corresponding to 2023–2039 has been estimated as being proportional to the production in the period 2020–June 2023. (**b**) Distribution among categories in the period 2020–June 2023: MSM: Materials Science Multidisciplinary; EEE: Engineering Electrical Electronic; PCM: Physics Condensed Matter; CM: Chemistry Multidisciplinary; PA: Physics Applied; NN: Nanoscience Nanotechnology; CP: Chemistry Physical; II: Instruments Instrumentation; O: Optics; CA: Chemistry Analytical.

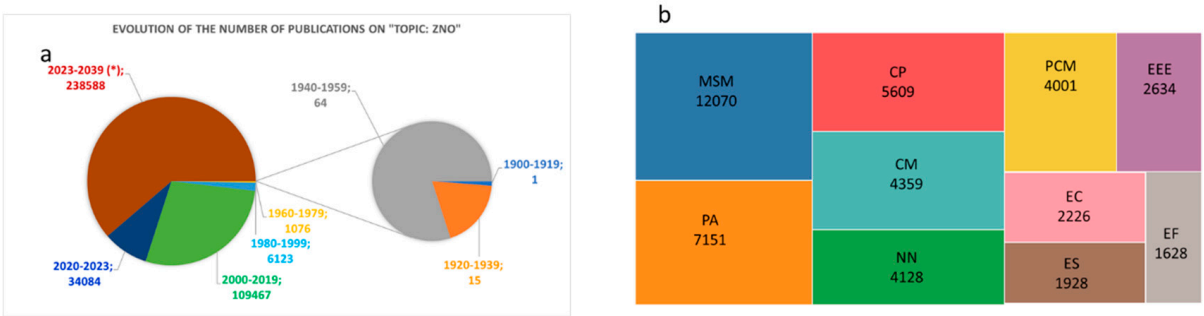

Figure 3. (**a**) Number of publications according to Web of Science Data Base on the search term "ZnO" from 1900 to date. * The number corresponding to 2023–2039 has been estimated as being proportional to the production in the period 2020–June 2023. (**b**) Distribution among categories in the period 2020–June 2023: MSM: Materials Science Multidisciplinary; EEE: Engineering Electrical Electronic; PCM: Physics Condensed Matter; CM: Chemistry Multidisciplinary; PA: Physics Applied; NN: Nanoscience Nanotechnology; CP: Chemistry Physical; EC: Engineering Chemical; ES: Environmental Sciences; EF: Energy Fuels.

ZnO has excellent properties in many different aspects, including the synergy between a wide band gap (3.37 eV), and a high concentration of native donor defects that makes ZnO one of the most widely studied Transparent Conductive Oxides (TCO). Another outstanding property is the large exciton binding energy (60 meV), which enables exciton-related transitions even at room temperature. Along with the above-mentioned properties, its chemical stability and some properties associated with the wurtzite structure (lack of a symmetry center) open the range of applications to technological fields as different as optoelectronics, gas sensing, photocatalysis, or piezoelectricity [24–29]. As observed in the distribution of publications per area, during the last decades, a new area, "Nanotechnology", arises and accumulates a large number of publications (Figures 1c, 2b and 3b). Then, it is worthy to have a look at the main factors present at the nano- and microscale, which further widen the scope for new applications [19,30–32]. Some of these factors include the enhancement of electroconductivity, a high specific area, and hence the role of surface and surface defect structure. On the other hand, the morphology of the structures plays a key role, and many of the properties of the material, for instance, luminescent properties, are strongly dependent on morphology [33–35].

One of the most relevant points in the field of semiconductors, particularly for semiconductor oxides, is the role of dopants to improve their properties. In fact, it is the primary route to modify and control most of their properties, especially, but not exclusively, their electrical and optical properties. The effect of dopants on the semiconductor material may be the direct supply of carriers, but also the modification of the defect structure, either native defects or impurities. On the other hand, the necessity to accommodate the dopant atoms into the host lattice may lead to the presence of extra stresses and/or relaxation phenomena that strongly influence the final defect structure. This not only includes point defects, but also extended defects such as dislocations, that may behave additionally as charge sinks or suppliers, due to the core disorder and the presence of broken or dangling bonds. For instance, in our focus material, ZnO, the conductivity increases up to 10 orders of magnitude due to the presence of impurities and native defects. An important drawback, in the particular case of ZnO, is the difficulty to obtain p-type material mainly due to self-compensation mechanisms [36–40]. A very good review on the p-type doping of ZnO can be found in [41].

Focusing on doped ZnO, Rare-Earth (RE) elements occupy a prominent position, and the number of studies of RE-doped ZnO-based systems with good luminescent properties has increased considerably [33,42–45]. Not all RE elements are used with the same purpose; for instance, in the case of Er, one major interest is in the telecom field due to the enhancement of the 1.54 μm emission [46–48]. However, the technological interest of RE doping goes beyond this field [49,50]. Lanthanides elements are characterized by an electronic structure of the form $[Xe]4f^n6s^2$. This means that they have a partially filled 4f shell shielded by the $5s^25p^6$ electrons. Optical transitions become then of the utmost importance. Three basic types of optical transitions may be observed: 4f–4f, 5d–4f, and the charge transfer between the host and the dopant. The 4f–5d transitions are allowed and have short lifetimes (in the order of ns). In addition, 5d orbitals are strongly affected by the crystal field and polarizability of the host material, which allows easy tuning in the visible region by changing some characteristics of the host ([22] and references therein). On the other hand, the f orbitals are shielded by the 5s and 5p; hence, they are not strongly influenced by the crystal field. Typically, they are responsible for very sharp transitions that extend over the whole wavelength range (from UV to IR). Nevertheless, the 4f-4f transitions are forbidden by the quantum selection rules, which give much longer lifetimes (in the order of μs). At first sight, this is a drawback if one of the main applications is the field of optoelectronics. However, by choosing the proper host (as ZnO for instance), the influence of the ligand field or non-centrosymmetric interactions may lead to a relaxation of the parity rule, and hence, to sharp emission lines that otherwise would not appear [51,52]. Having this in mind, it is clear that a major goal is the enhancement of the intensity of the luminescence emission.

Many efforts have been made to improve luminescent properties without deleterious sideband effects. We will only refer briefly to two of the basic approaches: the use of a sensitizer and the modification of the host lattice. In the first case, a suit sensitizer, i.e., a very effective radiation absorber that can transfer energy to the lanthanide ion, is introduced in the material, typically as a codopant. The second approach focuses on the modification of the host lattice so that, as previously mentioned, the parity rules are relaxed, favoring the transitions at lanthanide ions. For this purpose, Li^+ is commonly used [42,52,53]. Nevertheless, one of the main problems that we can face when doping with lanthanides is the mismatch between ionic radii (see Table 2) and the charge unbalance (the most frequently used are the RE trivalent ions). For these reasons, the effective doping of ZnO with rare elements is still challenging, although codoping strategies are a very good option [52,54–57].

Nevertheless, the main goal of this paper is to highlight the relevance gained in the last years by semiconductor oxides. Since many of the most recent applications that have been developed or are under development refer to optoelecronic properties, doping with rare earth elements has a central role. This was the reason behind choosing the system ZnO doped with Rare Earth elements (Eu, Gd, and Ce) and codoped with Ru to illustrate the materials' tuning potential of doping processes. In the following sections, we will describe the experimental details and the most remarkable aspects of the morphology, crystal structure, and luminescent properties of the systems studied. In Supplementary Information, files can be found concerning the revision of the works of the research group on ZnO-based systems.

2. Experimental

The synthesis of the samples has been carried out by the polyol method. It is a simple low-temperature liquid synthesis method that allows the synthesis of nanostructured particles of both a ceramic and metallic nature or a core-shell type. It allows good control in shape, size, composition, and crystallinity. In the conventional synthesis process, an EG (ethylene glycol)/DEG (diethylene glycol) medium, to which the controlling agents of the growth process (PVP-polyvinylpyrrolidone or urea) are added, is used. To ensure solubility in the reaction medium, acetates or nitrates of the desired metals are used.

Zinc acetate dihydrate ($Zn(CH_3COO)_2 \bullet 2H_2O$, purity > 98%, Sigma-Aldrich, Merck Life Science S.L.U., Madrid Spain) was used as a zinc precursor. The precursors used for the different dopants are indicated in Table 2.

Polyvinylpyrrolidone-PVP ($(C_6H_9NO)_n$, M_w = 40,000 g/mol, Sigma-Aldrich, Merck Life Science S.L.U., Madrid, Spain) and Ethylene glycol-EG ($C_2H_6O_2$, purity > 99.9%, Sigma-Aldrich, Merck Life Science S.L.U., Madrid, Spain) were added as a capping agent and solvent, respectively. All the precursor chemicals were reagent grade, and therefore, no further purifications were applied.

The reaction medium is heated up to 190 °C (for EG) in a controlled manner, avoiding any partial precipitation or change in the transparency of the solution. When temperatures close to the corresponding boiling points are reached, a change occurs in the liquid reaction medium, passing from a transparent to milky solution, after which the reaction is maintained for 1 h. The mixture is then allowed to cool to room temperature under constant stirring and the white precipitated solid is separated from the liquid medium. The nanoparticles are subjected to a centrifugation process to separate them from the medium by centrifugation (6000 rpm) and subjected to successive washes with ethanol and water mixtures. The powder was then dried in an oven at 90 °C for 12 h in air. A post-thermal treatment at 500 °C for 3 h was also used to increase the crystallinity of as-prepared powders.

With this synthesis mechanism, different samples with a fixed percentage of a rare earth element as the main dopant (2% wt) and a transition metal (Ru) as the codopant (0.25% wt) have been synthesized. Tables 1 and 2 summarize the composition/notation of the samples and dopant precursors used, respectively.

Table 1. Composition and notation of the samples.

Main Dopant (2% wt)	Codopant (0.25% wt)	Name
Ce	None	1CE
Gd		1GD
Eu		1EU
Ce	Ru	1CERU
Gd		1GDRU
Eu		1EURU

Table 2. Precursors.

Cation	Precursor	Supplier	CAS Number
Ce	$Ce(CH_3CO_2)_3 \bullet H_2O$	Sigma-Aldrich	206996-60-3
Gd	$Gd(NO_3)_3 \bullet 6H_2O$	Sigma-Aldrich	19598-90-4
Eu	$Eu(NO_3)_3 \bullet 5H_2O$	Sigma-Aldrich	63026-01-7
Ru	$RuCl_3 \bullet xH_2O$	Sigma-Aldrich	14898-67-0

Table 3 collects the ionic radii of the different cations in VI coordination (the most likely for the wurtzite structure), and the radii are expressed in Angstroms.

Table 3. Ionic radii for the cations in VI coordination.

	Cation	Charge	Crystal Radius	Ionic Radius
Host	Zn	2	0.88	0.74
TM	Ru	3	0.82	0.68
		4	0.76	0.62
		5	0.705	0.565
RE	Ce	3	1.15	1.01
		4	1.01	0.87
	Eu	2	1.31	1.17
		3	1.087	0.947
	Gd	3	1.078	0.938

The morphology, crystal structure, and luminescent properties of the samples have been investigated by Scanning Electron Microscopy (SEM), X-ray diffraction (XRD), Raman spectroscopy (RS), and μ-photoluminescence (μ-PL).

Scanning Electron Microscopy (SEM) has been carried out by means of an FEI Inspect S microscope (FEI Company, Hillsboro, OR, USA) operating at 15 kV.

X-ray diffraction experiments have been performed in a Philips X'Pert (Philips, Eindhoven, Netherlands), (40 kV, 40 mA) at the Cu K_α line (1.540598 Å). The maximum measurement range (2θ) was 20–80° with a scan step size of 0.02°/s.

Photoluminescence (PL) and Raman spectroscopy (RS) measurements have been performed in a confocal microscope (Horiba Jobin Yvon LabRAM HR800, Villeneuve d'Ascq, France) equipped with a He-Cd laser (λ = 325 nm) for PL measurements and a He-Ne laser (λ = 632.8 nm) for RS experiments. Both RS and PL measurements have been performed at room temperature.

3. Results and Discussion

The set of samples has been described in the experimental section in Tables 1 and 2. It consists of six samples, three of which are singly doped with 2% in weight of a rare earth (Ce, Eu, or Gd). This dopant content corresponds to the weight of the precursor (hydrated nitrates for Eu and Gd and hydrated carbonate for Ce). The other three samples in the set maintain the content in the rare earth element, but incorporate ruthenium as a second dopant. The precursor for Ru is hydrated chloride, and its weight percentage is 0.25%.

Referring to the singly doped samples, their morphology is very similar in all cases. Spherical or quasi-spherical nanoparticles that are quite homogeneous in size are observed. The particle sizes are between 12 and 15 nm, although in the case of the samples doped with Ce, a higher dispersion, with particles reaching up to 25 nm, and larger agglomerates are found.

Figure 4 shows Scanning Electron Microscopy images of typical samples in this set. As mentioned, only the Ce-doped samples (Figure 4a) show an appreciable size dispersion, and larger particles or agglomerates have been encircled to make this effect more visible. Figure 4b,c correspond to Eu- and Gd-doped samples, respectively. Similar areas to that in Figure 4a do not show agglomerates nor large particles. The addition of ruthenium as a codopant does not influence the morphology, although in the samples doped with Ce and Ru, a more homogeneous size distribution is observed in comparison to the samples doped with Ce only (Figure 4d). In Figure 4d, only a couple of larger agglomerates are observed in an area similar to that shown in Figure 4a.

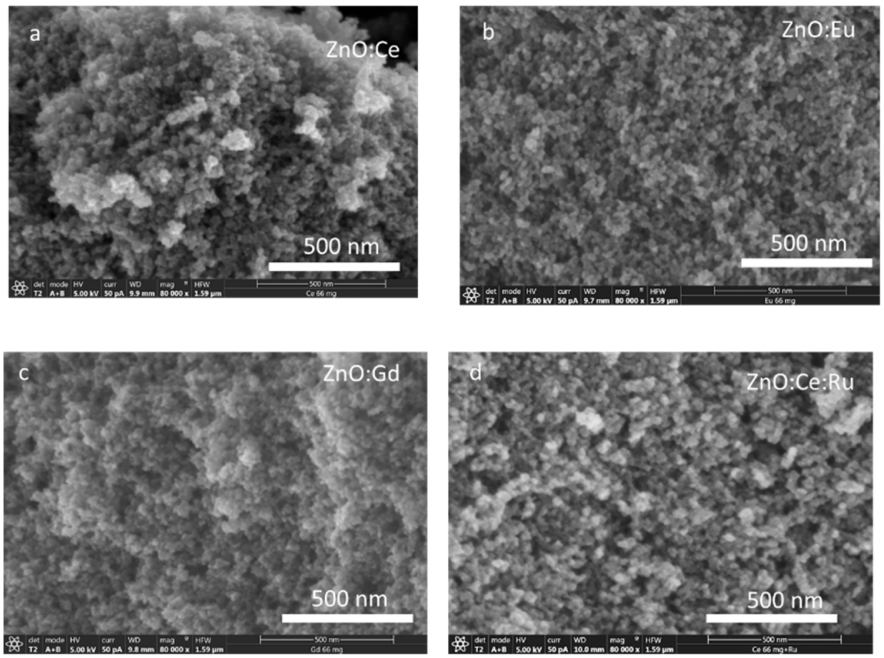

Figure 4. Scanning Electron images of (**a**) ZnO:Ce; (**b**) ZnO:Eu; (**c**) ZnO:Gd; (**d**) ZnO:Ce:Ru.

To investigate this point further, a zoom of the three most intense peaks is shown in Figure 6. These peaks correspond to the (100), (002), and (101) family planes.

As shown in Figure 5, X-ray diffraction experiments do not reveal the presence of second phases, hence suggesting that in all cases, the dopants are incorporated into the ZnO host lattice. As indicated in Figure 5, all the peaks may be indexed as corresponding to the wurtzite phase of ZnO (JCPDS-01-089-7102).

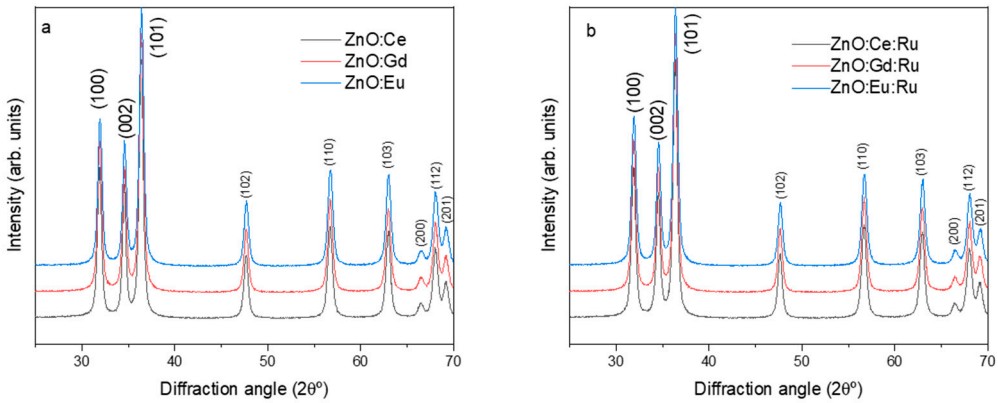

Figure 5. Comparison among the XRD spectra of: (**a**) Ce-, Eu-, and Gd-doped samples; (**b**) Ru-codoped samples.

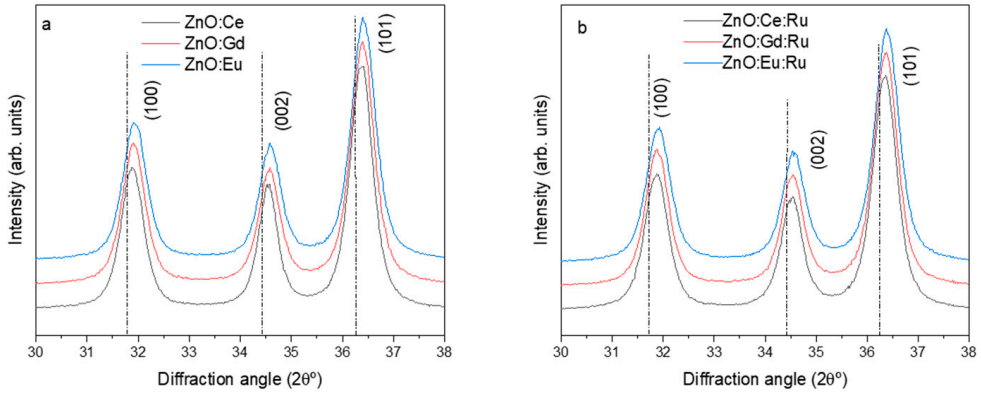

Figure 6. Zoom of the three main XRD peaks: (**a**) singly doped samples; (**b**) codoped samples.

Considering the ionic radii of Zn and dopant ions (Table 3), slight shifts towards lower angles would be expected, since all three ions, Ce^{+3}, Eu^{+3}, and Gd^{+3} (the most common valence state), in VI coordination (expected for the cations in the wurtzite structure) are larger than Zn^{+2} (see Table 3). Figure 6a,b show, respectively, the comparison among the singly doped samples (ZnO:RE) and the codoped samples (ZnO:RE:Ru). However, from this figure a shift towards larger angles is observed in all the samples, although it seems to be smaller upon Ru codoping. The black dotted line in this figure indicates the theoretical position of the diffraction peak according to the reference JCPDS card. From Bragg's law

$$2d_{hkl} sin\,\theta = \lambda$$

we can determine the interplanar distance corresponding to each plane family and then calculate the lattice parameters and the lattice volume (Figure 7). For a hexagonal lattice, the interplanar distance is written as

$$\frac{1}{d_{hkl}^2} = \frac{4}{3}\frac{h^2 + hk + k^2}{a^2} + \frac{l^2}{c^2}$$

which by selecting the data corresponding to the (100) and (002) peaks, lets us determine the lattice parameters a and c

$$\frac{1}{d_{hkl}^2} = \frac{4}{3}\frac{h^2 + hk + k^2}{a^2} + \frac{l^2}{c^2} \Longrightarrow \left\{ \begin{array}{c} \frac{1}{d_{100}^2} = \frac{4}{3}\frac{1}{a^2} \\ \frac{1}{d_{002}^2} = \frac{4}{c^2} \end{array} \right\}$$

and the cell volume may be determined from the expression

$$V = \frac{\sqrt{3}}{2} a^2 c$$

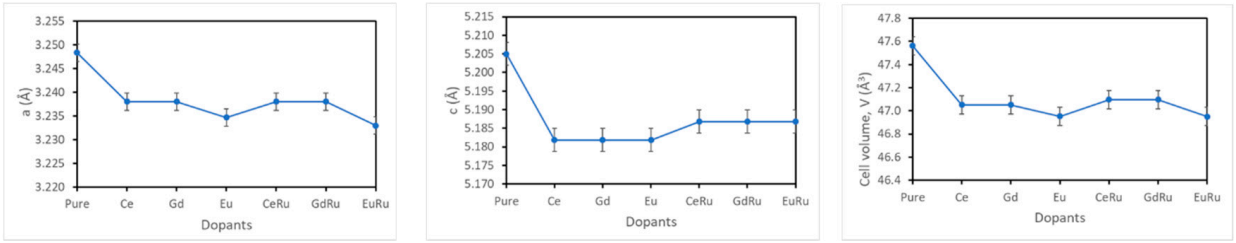

(**a**) (**b**) (**c**)

Figure 7. Comparison of lattice parameters: (**a**) a parameter; (**b**) c parameter; (**c**) volume cell.

As observed in Figure 7, the main differences occur along the z axis, although a decrease in the lattice parameter a is also appreciated. As mentioned according to the ionic radii difference, the behavior should be the opposite, however the charge difference could also play an important role. The most common charge state for the RE elements used in this work is +3, while that for Zn is +2, and hence, the electrostatic potential between the RE cation and the O anion would be higher than that between Zn and O. This could give rise to a decrease in the bond length and then a reduction in the cell volume that would compete with the expected increase associated with the larger ionic radius. As seen in the plots in Figure 7, the difference between the different dopants is within the error interval, which on the other hand is not surprising since the charge state of all three RE dopants is the same and the ionic radii are not very different. The introduction of Ru as a codopant seems to be the opposite, i.e., a very slight increase in the lattice parameters in respect to the singly doped samples. However, as previously mentioned, the differences fall within the calculation error and should not be taken into account.

On the other hand, the Raman spectra do not indicate the presence of high stresses, and no appreciable shifts or a remarkable broadening are observed in the Raman peaks. As an example, in Figure 8, the Raman spectra of the samples 1GD and 1GDRU are shown. The most intense peaks correspond to those of ZnO, which again is an indication that no second phases associated with doping are present. They are ascribed to the E_2^{low} (97 cm^{-1}) and E_2^{high} (436 cm^{-1}), in agreement with the values usually reported [58].

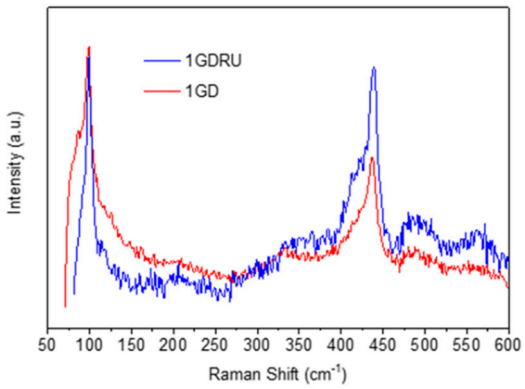

Figure 8. Raman spectra of ZnO.Gd and ZnO:Gd:Ru samples.

Finally, we present some results on photoluminescence. In all the samples, the photoluminescence spectra consist of the two main bands typically observed in ZnO: Near Band Edge (NBE), including band-to-band and shallow level related transitions, peaking

around 390nm, and a broad band in the visible region that results from the contributions of the different Deep Level transitions associated with defects and in the RE-doped samples, intraionic emissions. However, important differences among the samples are encountered (Figure 9). A deconvolution of this broad band has been made assuming gaussian profiles, and the NBE emission may be decomposed in three components: 380 nm (3.26 eV), 397 nm (3.12 eV), and 418 nm (2.97 eV). All three components are present in all the samples; however, its relative intensity is different, causing the apparent shift of the emission. This effect is much clearer when comparing each sample with the corresponding codoping with Ru, as we will discuss later. The structure of the DL emission is very complex. At least five components are involved, giving a very broad band that extends practically over the whole visible range: 520 nm (2.38 eV), 540 nm (2.30 eV), 560 nm (2.21 eV), 606 nm (2.05 eV), and 636 nm (1.95 eV). These components are related to several defects as O_{Zn}, oxygen vacancy-related (V_oZn_i, V_O, and V_O^+) or oxygen interstitials [59–61]. Regardless of the defects present, in the Eu-doped samples, intraionic transitions fall into the range from 420 to 656 nm (1.89−2.96 eV) [43]. The photoluminescence spectra show that in all cases, a decrease in emission intensity is observed upon Ru introduction (Figure 9b–d). As mentioned above, besides the reduction in the emission intensity, the most remarkable changes refer to the shifts observed in the Near Band Edge and in the relative intensities of the NBE and DL bands. It should be noted that the band edge emission in the samples containing Ce and Gd is shifted towards the blue zone due to the greater weight of the longer wavelength components. This effect is clearer in the sample doped with Ce (Figure 9b), as the emission maximum of the sample codoped with Ce and Ru coincides with the position of the shoulder observed in the sample doped with Ce. In the sample doped with europium, the most intense component is the one with the longest wavelength (approx. 420 nm), which as mentioned above, could have a contribution of the intraionic emissions $^5D_3 \rightarrow {}^7F_0$, with several lines in the range 2.79–2.96 eV [43].

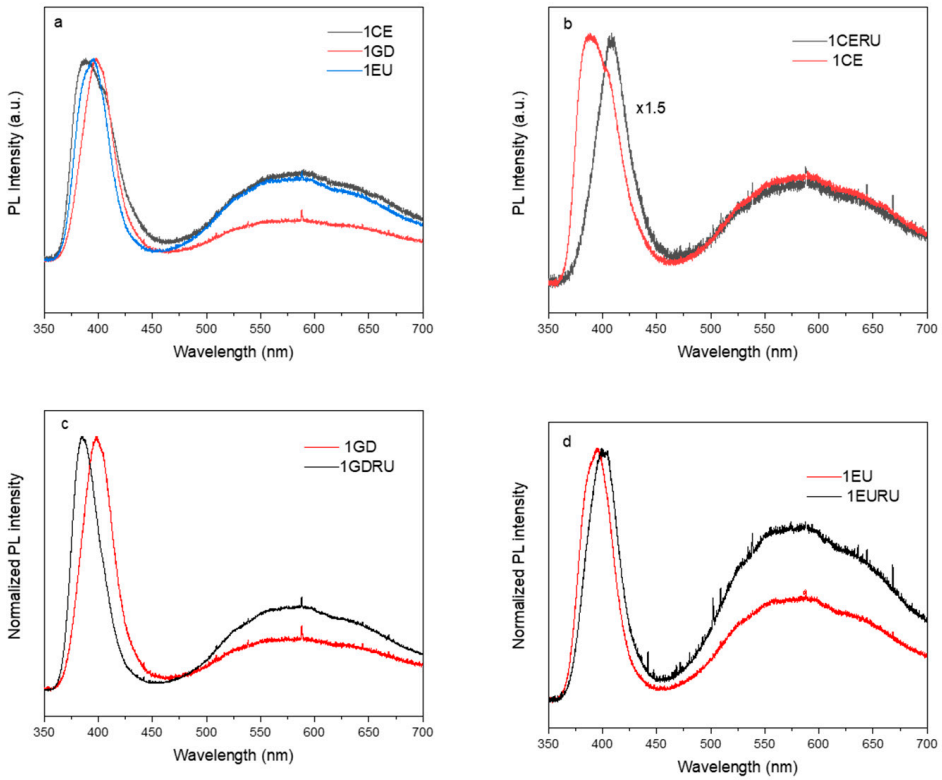

Figure 9. Photoluminescence spectra of doped and codoped samples. (**a**) Singly doped samples; (**b**) Ce doped and Ce/Ru coped samples; (**c**) Gd doped and Gd/Ru coped samples; (**d**) Eu doped and Eu/Ru coped samples.

4. Conclusions

ZnO has demonstrated to be one of the most versatile systems. According to the data presented in this work (extracted from the Web of Science Data Base), in the period 1920–1939, the works published on ZnO appeared to be categorized in six different areas, already with the next period considered (1940–1959) and ten areas listed. The number of categories and the categories themselves are a clear indication of the potential and versatility of this material, and may serve to follow the rise of new applications. In Supplementary Information, Files S2 include graphs with the distribution of published papers from 1900 to date. Besides those that could be considered basic areas such as Physics of Condensed Matter, Materials Science, or Chemistry Physical, in the period 1940–1979, areas such as Materials Science Ceramics accumulate a good number of publications. This is the period in which many of the basic studies on varistors were conducted. In the last two periods considered, Physics Applied and Materials Science Multidisciplinary accumulate the largest number of publications, however, Nanoscience and Nanotechnology (always restricted to ZnO) reaches more than 15,000 papers, and the areas more closely related to technological applications and Electrical Engineering and Electronics of Fuel Energy are also relevant. It is interesting to observe that during the first periods considered, the areas accumulating the largest number of papers were closer to Chemistry (Chemistry Multidisciplinary and Chemistry Physical), but evolved to areas closer to Physics (Physics Applied or Physics Condensed Matter) to finally observe Materials Science Multidisciplinary as the most prominent area, reflecting the ever more diffuse frontier between Physics and Chemistry.

The experimental results on the system ZnO:RE and ZnO:RE:Ru are only an example of the possibilities that ZnO offers to modify its properties with small amounts of dopant elements, and the influence on defect structure and the possible effects on the lattice have been described. In Supplementary Information, Files S1 purely research works of this group and in them, a good literature revision may be found.

Supplementary Materials: The following supporting information can be downloaded at: https://www.mdpi.com/article/10.3390/photonics10101106/s1, Supplementary Information: Literature revision and full set of bibliometric figures.

Author Contributions: J.F.R.-J.: formal analysis, original draft; A.F.: original draft, investigation, and methodology; G.F.-C.: investigation, formal analysis; S.R.-C.: experimental investigation; A.U.: investigation, formal analysis, and writing—review and editing; P.F.: investigation, formal analysis, supervision, and writing—review and editing; M.E.R.: investigation, formal analysis, supervision, and writing—review and editing. All authors have read and agreed to the published version of the manuscript.

Funding: This work has been financially supported by Comunidad de Madrid, Spain (S2018/NMT-4411), by the Integracion de Redes Temáticas de San Luis de Potosi (BUAP-CA-275) and Ministry of Economia, Industría y Competividad (PID2019-106631GB-C43).

Institutional Review Board Statement: Not applicable.

Informed Consent Statement: Not applicable.

Data Availability Statement: Research data will be available upon request to the corresponding author (arana@ucm.es).

Acknowledgments: This work has been financially supported by Comunidad de Madrid, Spain (S2018/NMT-4411), by the Integracion de Redes Temáticas de San Luis de Potosi (BUAP-CA-275) and Ministry of Economia, Industría y Competividad (PID2019-106631GB-C43).

Conflicts of Interest: The authors declare no conflict of interest.

References

1. Zhu, L.; Zeng, W. Room-temperature gas sensing of ZnO-based gas sensor: A review. *Sens. Actuators A Phys.* **2017**, *267*, 242–261. [CrossRef]
2. Yuan, S.; Duan, X.; Liu, J.; Ye, Y.; Lv, F.; Liu, T.; Zhang, X. Recent progress on transition metal oxides as advanced materials for energy conversion and storage. *Energy Storage Mater.* **2021**, *42*, 317–369. [CrossRef]
3. Samadi, M.; Zirak, M.; Naseri, A.; Khorashadizade, E.; Moshfegh, A.Z. Recent progress on doped ZnO nanostructures for visible-light photocatalysis. *Thin Solid Films* **2016**, *605*, 2–19. [CrossRef]
4. Tuller, H.L.; Bishop, S.R. Point Defects in Oxides: Tailoring Materials Through Defect Engineering. *Annu. Rev. Mater. Res.* **2011**, *41*, 369–398. [CrossRef]
5. Nikolic, M.V.; Milovanovic, V.; Vasiljevic, Z.Z.; Stamenkovic, Z. Semiconductor Gas Sensors: Materials, Technology, Design, and Application. *Sensors* **2020**, *20*, 6694. [CrossRef] [PubMed]
6. Monk, P.M.S.; Mortimer, R.J.; Rosseinsky, D.R. Metal Oxides. *Electrochromism* **1995**, *10*, 59–92. [CrossRef]
7. Ong, C.B.; Ng, L.Y.; Mohammad, A.W. A review of ZnO nanoparticles as solar photocatalysts: Synthesis, mechanisms and applications. *Renew. Sustain. Energy Rev.* **2018**, *81*, 536–551. [CrossRef]
8. Yu, X.; Marks, T.J.; Facchetti, A. Metal oxides for optoelectronic applications. *Nat. Mater.* **2016**, *15*, 383–396. [CrossRef]
9. Wetchakun, K.; Samerjai, T.; Tamaekong, N.; Liewhiran, C.; Siriwong, C.; Kruefu, V.; Wisitsoraat, A.; Tuantranont, A.; Phanichphant, S. Semiconducting metal oxides as sensors for environmentally hazardous gases. *Sens. Actuators B Chem.* **2011**, *160*, 580–591. [CrossRef]
10. Seshadri, R. Oxide Crystal Structures: The Basics. 2020. Available online: https://www.mrl.ucsb.edu/~seshadri/2015_218/OxidesStructures-BVS.pdf (accessed on 25 September 2023).
11. Yoon, Y.; Truong, P.L.; Lee, D.; Ko, S.H. Metal-Oxide Nanomaterials Synthesis and Applications in Flexible and Wearable Sensors. *ACS Nanosci. Au* **2022**, *2*, 64–92. [CrossRef]
12. Charles, V.L.P.; Crowther, W.H. Preparation and Properties of Zinc Oxide and Cadmium Oxide. *J. Am. Chem. Soc.* **1917**, *39*, 1046–1063.
13. Haga, Y.; Haga, E. Ueber die Lumineszenz des Zinkoxyds. *Phys. Z.* **1922**, *23*, 98–104.
14. Cooper, J.R.; Rhoderick, E.H. Copper-doped zinc oxide—A new room-temperature varistor. *J. Phys. D Appl. Phys.* **1967**, *1*, 493–496.
15. Ozgür, Ü.; Alivov, Y.I.; Liu, C.; Teke, A.; Reshchikov, M.A.; Doğan, S.; Avrutin, V.; Cho, S.-J.; Morkoç, H. A comprehensive review of ZnO materials and devices. *J. Appl. Phys.* **2005**, *98*, 041301. [CrossRef]
16. Kumari, P.; Misra, K.P.; Chattopadhyay, S.; Samanta, S. A brief review on transition metal ion doped ZnO nanoparticles and its optoelectronic applications. *Mater. Today Proc.* **2021**, *43*, 3297–3302. [CrossRef]
17. Kumar, R.; Al-Dossary, O.; Kumar, G.; Umar, A. Zinc Oxide Nanostructures for NO_2 Gas–Sensor Applications: A Review. *Nano-Micro Lett.* **2015**, *7*, 97–120. [CrossRef] [PubMed]
18. Singh, P.; Kumar, R.; Singh, R.K. Progress on Transition Metal-Doped ZnO Nanoparticles and Its Application. *Ind. Eng. Chem. Res.* **2019**, *58*, 17130–17163. [CrossRef]
19. Daksh, D.; Agrawal, Y.K. Rare Earth-Doped Zinc Oxide Nanostructures: A Review. *Rev. Nanosci. Nanotechnol.* **2016**, *5*, 1–27. [CrossRef]
20. Kumar, S.G.; Kavitha, R.; Sushma, C. Doped zinc oxide nanomaterials: Structure–electronic properties and photocatalytic applications. 2020, 31, 285–312. *Interface Sci. Technol.* **2020**, *31*, 285–312. [CrossRef]
21. Bhati, V.S.; Hojamberdiev, M.; Kumar, M. Enhanced sensing performance of ZnO nanostructures-based gas sensors: A review. *Energy Rep.* **2020**, *6*, 46–62. [CrossRef]
22. Bong, H.-Y.; Umar, A. *Metal Oxide Nanostructures and Their Applications*; American Scientific Publishers: Valencia, CA, USA, 2010.
23. Ahmad, M.; Zhu, J. ZnO based advanced functional nanostructures: Synthesis, properties and applications. *J. Mater. Chem.* **2011**, *21*, 599–614. [CrossRef]
24. Wang, Z. Novel nanostructures of ZnO for nanoscale photonics, optoelectronics, piezoelectricity, and sensing. *Appl. Phys. A* **2007**, *88*, 7–15. [CrossRef]
25. Kołodziejczak-Radzimska, A.; Jesionowski, T. Zinc Oxide—From Synthesis to Application: A Review. *Materials* **2014**, *7*, 2833–2881. [CrossRef] [PubMed]
26. Skompska, M.; Zarębska, K. Electrodeposition of ZnO Nanorod Arrays on Transparent Conducting Substrates–a Review. *Electrochim. Acta* **2014**, *127*, 467–488. [CrossRef]
27. Wang, Z.L. ZnO nanowire and nanobelt platform for nanotechnology. *Mater. Sci. Eng. R Rep.* **2009**, *64*, 33–71. [CrossRef]
28. Ajmal, H.M.S.; Khan, F.; Huda, N.U.; Lee, S.; Nam, K.; Kim, H.Y.; Eom, T.-H.; Kim, S.D. High-Performance Flexible Ultraviolet Photodetectors with Ni/Cu-Codoped ZnO Nanorods Grown on PET Substrates. *Nanomaterials* **2019**, *9*, 1067. [CrossRef]
29. Ajmal, H.M.S.; Khan, F.; Nam, K.; Kim, H.Y.; Kim, S.D. Ultraviolet Photodetection Based on High-Performance Co-Plus-Ni Doped ZnO Nanorods Grown by Hydrothermal Method on Transparent Plastic Substrate. *Nanomaterials* **2020**, *10*, 1225. [CrossRef]
30. Ronning, C.; Gao, P.X.; Ding, Y.; Wang, Z.L.; Schwen, D. Manganese-doped ZnO nanobelts for spintronics. *Appl. Phys. Lett.* **2004**, *84*, 783–785. [CrossRef]

31. Willander, M.; Nur, O.; Bano, N.; Sultana, K. Zinc oxide nanorod-based heterostructures on solid and soft substrates for white-light-emitting diode applications. *New J. Phys.* **2009**, *11*, 125020. [CrossRef]
32. Willander, M.; Nur, O.; Sadaf, J.R.; Qadir, M.I.; Zaman, S.; Zainelabdin, A.; Bano, N.; Hussain, I. Luminescence from Zinc Oxide Nanostructures and Polymers and their Hybrid Devices. *Materials* **2010**, *3*, 2643–2667. [CrossRef]
33. Singh, P.; Singh, R.K.; Kumar, R. Journey of ZnO quantum dots from undoped to rare-earth and transition metal-doped and their applications. *RSC Adv.* **2021**, *11*, 2512–2545. [CrossRef] [PubMed]
34. Ariza, R.; Pavón, F.; Urbieta, A.; Fernández, P. Study of the influence of dopant precursor on the growth and properties of Li-doped ZnO. *J. Phys. Chem. Solids* **2020**, *139*, 109354. [CrossRef]
35. Urbieta, A.; Fernández, P.; Piqueras, J. Nanowires and stacks of nanoplates of Mn doped ZnO synthesized by thermal evaporation-deposition. *Mater. Chem. Phys.* **2012**, *132*, 1119–1124. [CrossRef]
36. Galli, G. Solid-state physics: Doping the undopable. *Nature* **2005**, *436*, 32–33. [CrossRef]
37. Zhang, S.B.; Wei, S.-H.; Zunger, A. Microscopic Origin of the Phenomenological Equilibrium "Doping Limit Rule" in *n*-Type III-V Semiconductors. *Phys. Rev. Lett.* **2000**, *84*, 1232–1235. [CrossRef]
38. Tang, K.; Gu, S.-L.; Ye, J.-D.; Zhu, S.-M.; Zhang, R.; Zheng, Y.-D. Recent progress of the native defects and p-type doping of zinc oxide. *Chin. Phys. B* **2017**, *26*, 047702. [CrossRef]
39. Avrutin, V.; Silversmith, D.J.; Morkoç, H. Doping Asymmetry Problem in ZnO: Current Status and Outlook. *Proc. IEEE* **2010**, *98*, 1269–1280. [CrossRef]
40. Yan, Y.; Wei, S.-H. Doping asymmetry in wide-bandgap semiconductors: Origins and solutions. *Phys. Status Solidi (b)* **2008**, *245*, 641–652. [CrossRef]
41. Fan, J.; Sreekanth, K.; Xie, Z.; Chang, S.; Rao, K. p-Type ZnO materials: Theory, growth, properties and devices. *Prog. Mater. Sci.* **2013**, *58*, 874–985. [CrossRef]
42. Pal, P.P.; Manam, J. Enhanced luminescence of ZnO:RE3+ (RE=Eu, Tb) nanorods by Li+ doping and calculations of kinetic parameters. *J. Lumin.* **2014**, *145*, 340–350. [CrossRef]
43. Zhong, Tian and Philippe Goldner, Emerging rare-earth doped material platforms for quantum nanophotonics. *Nanophotonics* **2019**, *8*, 2003–2015. [CrossRef]
44. Gaggero, E.; Calza, P.; Cerrato, E.; Paganini, M.C. Cerium-, Europium- and Erbium-Modified ZnO and ZrO 2 for Photocatalytic Water Treatment Applications: A Review. *Catalysts* **2021**, *11*, 1520. [CrossRef]
45. Kumar, V.; Ntwaeaborwa, O.M.; Soga, T.; Dutta, V.; Swart, H.C. Rare Earth Doped Zinc Oxide Nanophosphor Powder: A Future Material for Solid State Lighting and Solar Cells. *ACS Photon.* **2017**, *4*, 2613–2637. [CrossRef]
46. Ryu, Y.K.; Fernández, P.; Piqueras, J. Growth and characterization of Er-doped ZnO elongated nanostructures. *Phys. Status Solidi (a)* **2011**, *208*, 868–873. [CrossRef]
47. Fan, R.; Lu, F.; Li, K. Single-mode channel waveguide at 1540 nm in Er-doped ZnO thin film. *J. Lumin.* **2017**, *192*, 410–413. [CrossRef]
48. Lo, J.-W.; Lin, C.-A.; He, J.-H. Er-Doped ZnO Nanorod Arrays with Enhanced IR Emission by Using Au Island Films. *Curr. Nanosci.* **2011**, *7*, 282–287. [CrossRef]
49. Kenyon, A. Recent developments in rare-earth doped materials for optoelectronics. *Prog. Quantum Electron.* **2002**, *26*, 225–284. [CrossRef]
50. Zhou, Z.-Q.; Liu, C.; Li, C.-F.; Guo, G.-C.; Oblak, D.; Lei, M.; Faraon, A.; Mazzera, M.; de Riedmatten, H. Photonic Integrated Quantum Memory in Rare-Earth Doped Solids. *Laser Photonics Rev.* **2023**, 2300257. [CrossRef]
51. Eliseeva, S.V.; Bünzli, J.C. Lanthanide luminescence for functional materials and bio-sciences. *Chem. Soc. Rev.* **2010**, *39*, 1–380. [CrossRef]
52. Singh, A.K.; Singh, S.K.; Rai, S.B. Role of Li^+ion in the luminescence enhancement of lanthanide ions: Favorable modifications in host matrices. *RSC Adv.* **2014**, *4*, 27039–27061. [CrossRef]
53. Krishna, R.; Haranath, D.; Singh, S.P.; Chander, H.; Pandey, A.C.; Kanjilal, D. Synthesis and improved photoluminescence of Eu:ZnO phosphor. *J. Mater. Sci.* **2007**, *42*, 10047–10051. [CrossRef]
54. Khanum, R.; Das, N.M.; Moirangthem, R.S. Defect engineered ZnO whispering gallery modes via doping with alkali metal ions for label-free optical sensors. *J. Appl. Phys.* **2019**, *125*, 173107. [CrossRef]
55. Ariza, R.; Sotillo, B.; Pavón, F.; Urbieta, A.; Fernández, P. Evolution of Whispering Gallery Modes in Li-Doped ZnO Hexagonal Micro- and Nanostructures. *Appl. Sci.* **2020**, *10*, 8602. [CrossRef]
56. Pavón, F.; Urbieta, A.; Fernández, P. Luminescence and light guiding properties of Er and Li codoped ZnO nanostructures. *J. Lumin.* **2018**, *195*, 396–401. [CrossRef]
57. Pavón, F.; Ariza, R.; Urbieta, A.; Fernández, P. Morphology, Luminescence, and Optical Properties of Tb- and Li-Codoped ZnO Elongated Nano- and Microstructures. *Phys. Status Solidi (a)* **2022**, *219*. [CrossRef]
58. Cuscó, R.; Alarcón-Lladó, E.; Ibáñez, J.; Artús, L.; Jiménez, J.; Wang, B.; Callahan, M.J. Temperature dependence of Raman scattering in ZnO. *Phys. Rev. B* **2007**, *75*, 165202. [CrossRef]
59. Vempati, S.; Mitra, J.; Dawson, P. One-step synthesis of ZnO nanosheets: A blue-white fluorophore. *Nanoscale Res. Lett.* **2012**, *7*, 470. [CrossRef]

60. Kumar, V.; Prakash, J.; Pathak, D.; Sharma, D.P.; Purohit, L.P.; Swart, H.C. Ion beam engineering of implanted ZnO thin films for solar cell and lighting applications. *Chem. Eng. J. Adv.* **2023**, *15*, 100501. [CrossRef]
61. Galdámez-Martinez, A.; Santana, G.; Güell, F.; Martínez-Alanis, P.R.; Dutt, A. Photoluminescence of ZnO Nanowires: A Review. *Nanomaterials* **2020**, *10*, 857. [CrossRef]